POLITECNICO
MILANO 1863

SCUOLA DI INGEGNERIA INDUSTRIALE
E DELL'INFORMAZIONE

Executive Summary of the Thesis

Magnetic switching of Ta/CoFeB/MgO heterostructures via Spin Orbit Torque for memory applications

Laurea Magistrale in Electronics Engineering - Ingegneria Elettronica

Author: Matteo Fettizio

Advisor: Prof. Riccardo Bertacco

Co-advisor: Dr. Luca Nessi

Academic year: 2021-2022

1. Introduction

Ferromagnets are materials that can present a net macroscopic magnetic moment even in the absence of an external magnetic field and this makes them suitable for the storage of digital information.
The first use of magnetism for data storage is the magnetic hard drive, used for secondary memories due to time consuming reading and writing processes.
The discoveries of giant magnetoresistance in 1988 by Fert [2] and of tunneling magnetoresistance in 1975 by Julliere [8] open new horizons for magnetic storage, allowing it to finally represent a competitive alternative to CMOS technology for the implementation of primary memories.
Magnetic tunnel junctions are the core of the "magnetoresistive random access memory" (MRAM), in which the two bits are associated to the two relative magnetization's direction of the two junction's magnetic layers.
While information can be accessed fast and efficiently by means of a resistance measurement, the writing process has presented a major challenge that limited scalability and devices endurance [4].
The discovery of Spin Orbit Torques (SOT) introduces a way to solve these issues, since it permits to write the magnetization of the cell injecting a current in a heavy metal layer placed underneath it [4]. Due to spin orbit interaction this current gets converted into a pure spin current which provides the magnetic momentum needed for switching.
Further improving scalability without affecting thermal stability is possible with the introduction of MRAM with perpendicular magnetic anisotropy (PMA). Of particular relevance is the observation of large PMA in CoFeB/Mgo heterostructures, when the CoFeB thickness is around 1nm, due to interfacial effects [3].
This system, in fact, not only provides PMA but it is also suitable for the realization of magnetic tunneling junction since, when grown on top of CoFeB, MgO can achieve the (001) texture needed to give rise to a high tunneling magnetoresistance (TMR). Finally, the presence of tantalum allows for SOT induced writing due to the high spin hall angle of its beta crystalline phase [6].
In conclusion, these are the reasons why the experimental work described in this thesis deals with the realization and characterization of

Ta/CoFeB/MgO/CoFeB/Ta based perpendicular magnetic tunneling junctions (pMTJ) and of SOT switching of Ta/CoFeB/MgO trilayers, with the future goal of integrating the results obtained in the final SOT-MRAM element.

2. Fabrication and characterization of magnetic tunnel junctions

In this section I describe the optimization of Ta/CoFeB/MgO/Ta pMTJsm where the bottom CoFeB acts as free layer and Ta as heavy metal performing the charge-to-spin conversion giving the SOT.
This is the first step towards the implementation of SOT-pMTJs for unconventional computing, which is the framework of this thesis.

2.1. Deposition and characterization of the magnetic stack

The magnetic properties of the heterostructure Ta(5)/Ru(10)/Ta(5)/CoFeB(1)/MgO(2) /CoFeB(1.4)/Ta(5)/Ru(5) are analyzed addressing separately the stack containing only the bottom and the top CoFeB layer.
The two structures are deposited by magnetron sputtering on thermally oxide silicon substrates and annealed under an out of plane (OOP) field of 300 mT at 250°C for one hour. Figure 1 shows the results of the OOP VSM measurement of the two films.

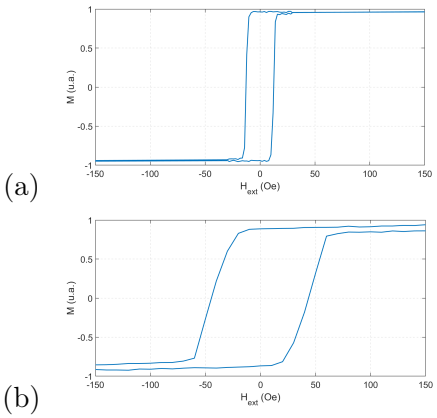

Figure 1: OOP hysteresis loop of the bottom layer structure (a) and of the top layer structure (b) after thermal annealing process.

Both layers present a squared loop indicating good PMA. Afterwards the full stack is deposited and annealed, showing the hysteresis loop of Figure 2.

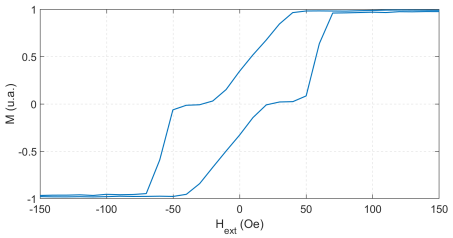

Figure 2: OOP hysteresis loop of the full magnetic structure after thermal annealing.

The distinct contributions of the two layers are visible, but while one preserves its PMA, the other shows a partially in plane anisotropy, as the first smooth magnetization reversal and the low remanent magnetization suggest.
By comparison with the cycles of the single layers it can be deduced that it is the bottom layer the one which loses its PMA character.
PMA gets spoiled only after the two layers are in the full structure. Weng *et al.* [9] report a loss of PMA in the bottom layer of the Ta/CoFeB/MgO/CoFeB/Ta heterorostructure as the annealing temperature grows over a certain threshold. This suggests that in the complete structure interdiffusion of tantalum, which is favoured by high temperatures, has a stronger influence over the magnetic properties of the system

2.2. Magnetic tunnel junctions fabrication

The fabrication consists on the sequence of 3 lithographic steps carried out using a lithographic mask already available in the research group.
First, the MESA structure, i.e. the area covered by the bottom contacts and by the channel containing the junction, is obtained via direct optical lithography and successive ion beam etching. AFM measurement is performed to quantify the thickness of the etched material (not shown).
The second step involves the definition of the magnetic pillars. Once again direct optical lithography and ion beam etching are carried out, while AFM is used to verify the correct outcome of the ecthing process. The thickness measured is compatible with the desired one, which is 14.4 nm.

In the lasts step the contacts are defined via inverse lithography and the stack Cr(10)/Cu(200) is deposited. A lift-off procedure is carried out to remove the metal outside the contacts regions. Figure 3 shows the optical microscopy view of a complete device

Figure 3: Microscope view of the result of the top contacts lift-off.

2.3. Electrical characterization

The first part of this subsection deals with I-V curves, for the verification of the tunneling nature of conduction, and with the evaluation of the R×A product among junctions with different areas. In the second part the dependence on the external magnetic field is explored with the measurements of tunneling magnetoresistance. All the experiments are carried out at room temperature.
The I-V curves are recorded in a four contacts configuration using a probe station on devices with different areas. While they all display the cubic trend compatible with tunneling transport, they do not possess a uniform R×A product.
A large TMR (evaluated as $\frac{R_{AP}-R_P}{R_P}$) is successfully observed in several devices over the sample, reaching the value of 98.4% in the devices whose R-H cycles is displayed in Figure 4.

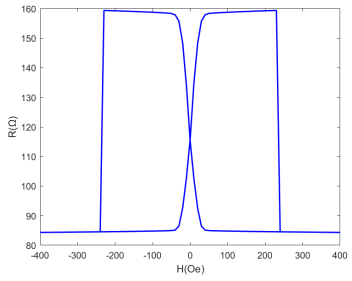

Figure 4: R-H cycles of two of the device having an elliptical pillar of 94.2 μm^2 area.

We can observe, in both R-H cycles, the sharp contribution given by the reversal of the top layer's magnetization and the smooth transition from parallel to antiparallel configuration given by the bottom layer, which has a weaker perpendicular anisotropy.

3. Fabrication and characterization of Hall bars for the investigation of SOT induced switching

In this section I discuss the results obtained from the experiments of SOT switching performed on Ta/CoFeB/MgO based Hall bars, in which we use anomalous Hall effect to probe the state of the out of plane magnetization measuring the transverse resistance R_{xy}.
Stacks with different Ta thicknesses (5nm, 10nm and 20nm) are used in order to find the conditions to obtain β-Ta which has a high spin-Hall angle θ_{SH} [10]. The devices layout is designed for the purpose and the fabrication involves three steps of mask-less alligned optical litography.

3.1. Dependence of SOT induced switching on tantalum's thickness

In this section the results of the measurements of SOT induced switching on devices with different tantalum's thicknesses will be shown and discussed.
The experiments performed are based on the one described in Ref. [7], in which the transverse resistance of the devices is measured under the application of a magnetic field of the following form with respect to the reference frame of Figure 5:

$$\boldsymbol{H}_{EXT} = (H_x, 0, H_z) \tag{1}$$

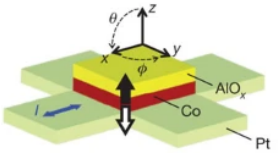

Figure 5: Pictorial representation of an Hall bar similar to the one used in our studies, taken from Ref. [7].

H_z is in the order of $\frac{H_x}{10}$ and it is required to

maintain the system oriented along z and prevent the formation of domains due to the large component along x [7]. H_x is required to alter the energy barrier for the up-to-down and down-to-up rotations, thus allowing deterministic switching [7].
The external field is swept between ± 5000 Oe and R_{xy} is measured for each value of the field both after a positive and a negative current pulse is injected in the device parallely to the field. SOT switching is detected when, for a given field, the two resistances are different.
Regarding the device with Ta thickness of 20 nm, the resistivity around 20 $\mu\Omega cm$ suggests tantalum is in α phase and therefore not adapt to induce SOT due to its small θ_{SH}.
The experiments, in fact, only show the reduction of the coercive field due to thermal activation induced by Joule heating.
The devices with Ta thickness of 5 nm show resistivity of around 200 $\mu\Omega cm$, compatible with β-Ta. However, we could not record reliable data regarding the SOT induced switching behaviour, since the device are not able to sustain the current pulses probably due to excessive tantalum's oxidation.
The sample with 10 nm thick tantalum finally allows to carry out successful SOT induced switching experiments. After surpassing the threshold density current of $1 \times 10^7 \frac{A}{cm^2}$, we observe the arising of two windows of positive and negative fields that allow current induced switching, whose width grows as the input current density grows. Figure 6 shows the outcome of the experiment carried out with the protocol described in Ref. [7] for pulses with current density of $1.6 \times 10^7 \frac{A}{cm^2}$.

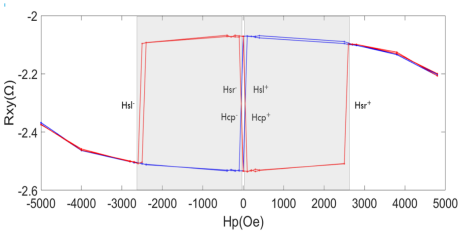

Figure 6: R_{xy}-H_p cycles with positive (blue curve) and negative (red curve) $1.6 \times 10^7 \frac{A}{cm^2}$ current density pulses. Dashed areas indicate the switching windows.

The same experiment is performed for current densities from 0 to $1.8 \times 10^7 \frac{A}{cm^2}$, with a step of $0.2 \times 10^7 \frac{A}{cm^2}$. The results are summarized in the phase diagram of Figure 7, in which the critical fields characterizing each R_{xy}-H_p cycle are associated to the value of current density at which they are recorded [7].

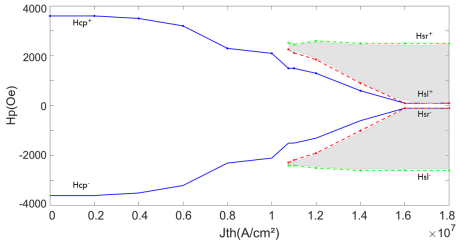

Figure 7: Phase diagram of the dependence of SOT switching on the input current density and H_p. The shaded regions between the red and green curves represent the switching windows.

3.2. Investigation of SOT induced switching asymmetry

This section presents the results of the SOT switching experiments collected from two devices having different types of dots, namely squared of 5 μm side and circular of 5 μm diameter, with particular attention given to the differences arising between the characteristics of SOT induced switching for positive and negative values of the external field.
The usual H-J phase diagrams (like that in Figure 7) are displayed in Figure 8a and Figure 8b for the circular and squared devices, respectively. In both diagrams the positive switching window is clearly larger than the negative one, meaning SOT switching is favoured for the former. The symmetric behaviour of the 10 μm circular device indicates that asymmetry is enhanced by reducing the devices' dimensions. Moreover, for the same size the squared device shows a more pronounced asymmetry than the circular one, suggesting a dependence of asymmetry on the dot's geometry.
This behaviour is compatible with the presence of an internal bias field pointing along the direction of the injected current, but further studies are necessary to clarify its origin.

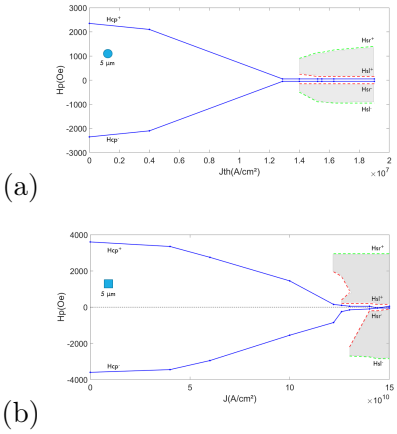

(a)

(b)

Figure 8: Phase diagram summarizing the dependence of SOT induced switching on the input current density and on the applied field for the circular device of 5 μm diameter(a) and for the squared device of μm side(b).

3.3. Dependence of SOT induced switching on the transverse applied field

The application of an external field H_y is expected to influence the spin orbit torques by adding up to the field-like effective field, which is directed in the y direction.

$$T_{FL} \propto \boldsymbol{M} \times \boldsymbol{y}; \quad H_{FL} \propto \boldsymbol{y} \tag{2}$$

In Ref. [5] is reported a shift of the R_{xy}-J hysteresis loops justified by the formula for the switching current density $j_c^{\pm}$ of a macrospin in presence of H_y and taking the field-like torque into account [5]. According to this equation, the sum between positive and negative threshold current densities is proportional to H_y.

$$j_c^+ + j_c^- \simeq \frac{eM_s t}{\hbar \xi_{DL} \beta} B_y \tag{3}$$

In order to evaluate the presence of the described behaviour, R_{xy}-J hysteresis cycles are recorded for different values of the ratio $\frac{H_y}{H_x}$ between -1 and +1 with a fixed H_x. The same experiment is repeated for different values of H_x, namely 1000 Oe, 1500 Oe, 2000 Oe. For each experiment, the quantity $j_c^+ + j_c^-$ is plotted against the relative H_y in Figure 9.

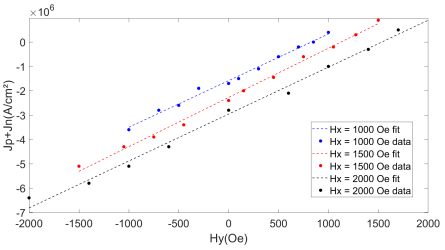

Figure 9: Data acquired and fitted curves relative to the dependence of sum between the positive and negative threshold current densities on H_y at fixed H_x of 1000 Oe (blue curve and points), 1500 Oe (black curve and points) and 2000 Oe (red curve and points) .

The three curves present similar slopes with an offset caused by a spurious H_z. We can use the average of the three, equal to $1.92 \times 10^4 \frac{A}{mTcm^2}$, to estimate $\xi_{FL} \simeq 14.8$. Scaling this value by two orders of magnitudes, which is the ratio between the threshold densities in microscopic and nanoscopic devices, gives a realistic value of ξ_{FL}, found equal to 0.11 in Ref. [5].

3.4. Attemp of realizing multistate switching tunable with Hy

In the landscape of devices for in-memory computing, memristors have gained large interest in the recent years, due to their potential to enable efficient brain-inspired computing.
The last part of the experimental work discussed in this thesis deals with the study of the possibility of using SOT to realize memristive switching in the fabricated Hall bars, following the approach of Ref. [1]. In addition, we explore the potentiality of using a transverse field to control intermediate states owing to the influence of H_y on the switching behaviour.
A sequence of trains of ten pulses of increasing amplitude is injected into the device and after each pulse the transverse resisted is recorded. For a given amplitude, train of pulses of both polarities are sent in order to toggle the state of the magnetization periodically.
In absence of transverse field the resistive response of the device shows only one intermediate state around 10.8 Ω in the transition from upper state to the lower one for current densities equal to $-1.29 \times 10^7 \frac{A}{cm^2}$ and $-1.33 \times 10^7 \frac{A}{cm^2}$ while no intermediate states are observed in the opposite transition. (Figure 10)

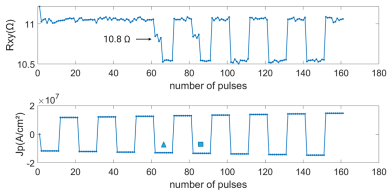

Figure 10: Time evolution of the transverse resistance of the device under study under the application of the described train pulses sequence. The pulses with the triangle and the square corresponds to current density of $-1.29 \times 10^7 \frac{A}{cm^2}$ and $-1.33 \times 10^7 \frac{A}{cm^2}$, respectively.

The addition of a transverse field has a different effect depending on its sign. A positive field introduces a new intermediate state at 10.9 Ω and shows a multistate switching only for negative pulses. A negative field only stabilizes the state at 10.8 Ω, which now appears only for positive pulses.

4. Conclusions

The Ta/CoFeB/MgO heterostructure has been employed for the fabrication of perpendicular magnetic tunnel junction and for the realization of deterministic Spin-Orbit Torque switching of out of plane magnetization.
Ta/CoFeB/MgO based Hall bars have been optimized in order to achieve deterministic Spin-Orbit Torque switching, with particular focus on the optimal thickness of the tantalum layer.
The dependences of the switching behaviour on the input current densities and on the external applied fields have been carefully addressed, highlighting the tendency of switching to be promoted or hindered when a positive or negative field collinear to the input current are applied, respectively. We ascribe this phenomenon to the presence of an internal biasing field, which may be caused by DMI. However, micromagnetic simulations are required to validate this hypothesis and to shed light on the influence of the geometrical properties of the device on the strength of this asymmetry.
Finally, an attempt to use SOT to induce intermediate states of the magnetization has been carried out. We discovered that a near-threshold working regime exists where two additional intermediate states arise and their occurance is influenced by the presence of an external field orthogonal to the direction of the injected current. In particular, these state are observed for positive or negative currents depending on whether the transverse field is negative or positive, respectively.
In conclusion, these studies open the possibility of developing new devices and concepts related to the field of emerging magnetic memories for digital storage and neuromorphic computing.

5. Acknowledgements

I want to thank Prof. Riccardo Bertacco, Luca Nessi and all the people at PoliFab that supported me during this experience.

References

[1] B Dieny *et al.*. Perpendicular magnetic anisotropy at transition metal/oxide interfaces and applications. *Reviews of modern physics, 89*, pages 025008–1—-025008–54, 2017.

[2] A. Fert *et al.*. Giant Magnetoresistance of (001)Fe/(001)Cr Magnetic Superlattices. *Physical Review Letters, 61*, pages 2472–2475, 1988.

[3] S Ikeda *et al.*. A perpendicular-anisotropy CoFeB–MgO magnetic tunnel junction. *Nature Materials 9*, pages 721–724, 2010.

[4] S Ikegawa *et al.*. Magnetoresistive Random Access Memory: Present and Future. *IEEE transaction on electron devices, 67(4)*, pages 1407–1419, 2020.

[5] V Krizakova *et al.*. Tailoring the switching efficiency of magnetic tunnel junctions by the fieldlike spin-orbit torque. *arXiv:2206.14587*, 2022.

[6] L Liu *et al.*. Spin-Torque Switching with the Giant Spin Hall Effect of Tantalum. *Science 336(6081)*, pages 555–558, 2012.

[7] I Mihai *et al.*. Perpendicular switching of a single ferromagnetic layer induced by in-plane current injection. *Nature, 476*, pages 189—-193, 2011.

[8] M.Julliere. Tunneling between ferromagnetic films. *Physics Letters A, 54(3)*, pages 225–226, 1975.

[9] Y Weng *et al.*. Interlayer Exchange Coupling and Perpendicular Magnetic Anisotropy in $Co_{40}Fe_{40}B_{20}$ /MgO/$Co_{20}Fe_{60}B_{20}$ Tunnel Junction Structures. *IEEE transactions on magnetics, 49*, pages 4425–4428, 2013.

[10] R Yu *et al.*. Determination of spin Hall angle and spin diffusion length in -phase-dominated tantalum. *Physical Review Materials 2(7)*, pages 074406–1–074406–7, 2004.